Impact of antenna design on MIMO performance for compact terminals with adaptive impedance matching

Vasilev, Ivaylo; Plicanic, Vanja; Lau, Buon Kiong

Published in:
IEEE Transactions on Antennas and Propagation

DOI:
10.1109/TAP.2016.2521885

2016

Document Version:
Peer reviewed version (aka post-print)

Impact of Antenna Design on MIMO Performance for Compact Terminals with Adaptive Impedance Matching

Ivaylo Vasilev, *Student Member*, *IEEE*, Vanja Plicanic, *Member*, *IEEE*, and Buon Kiong Lau, *Senior Member*, *IEEE*

***Abstract*—Using the metrics of channel capacity and multiplexing efficiency, the adaptive impedance matching (AIM) performances of two multiple-input multiple-output (MIMO) terminals with different antenna designs were evaluated and compared. The evaluation was performed in LTE Band 18 Downlink (860-875 MHz) under realistic usage conditions of two measured user handgrips and simulated propagation channels with different angular spreads (ASs). The results provide potential performance gains from AIM based on realistic MIMO terminal prototypes, and the underlying mechanisms by which the gains were achieved, which can serve as antenna and AIM circuit design guidelines. In particular, the evaluation revealed that ideal uncoupled AIM networks can increase the capacity by up to 52% relative to 50 ohm terminations. However, the observed gains depend heavily on the antenna design, the user scenario and the channel's angular spread. For example, the wideband design in different user cases experienced capacity gain of 4-9% from AIM in uniform 3D channels, in contrast to the 1.3-44% gain seen in a conventional narrowband design. In non-uniform channels with small ASs, the AIM gain for different mean incident angles depends on the absolute mean effective gain (MEG) and the change in correlation due to AIM; In cases where AIM has little impact on correlation, the mean incident angles with high AIM gains were close to those with high MEGs.**

***Index Terms*—MIMO systems, impedance matching, antenna measurements, handset antennas and multipath channels.**

I. Introduction

OVER the past decade, multiple-input multiple-output (MIMO) systems have become increasingly popular for both existing and upcoming wireless communication systems [1]. However, implementing efficient MIMO antennas in mobile terminals is very challenging, due to the terminals' compact form factor and the strong influence of users [2].

It is well known in antenna theory that impedance matching networks can be applied to maximize the transfer of power from the RF circuits to the antenna [3]. In the case of MIMO antennas, the matching networks can affect both impedance matching and mutual coupling, which can change the radiation patterns, efficiencies and bandwidths of the antenna elements, hence allowing some flexibility for the antennas to adapt to a given usage scenario. Therefore, optimizing the matching networks for better system performance has recently become an active field of research, where the focus has been on proof of concepts as well as verifications through simulations and measurements [4]-[15].

The possibility to use uncoupled matching networks to optimize received power and correlation was demonstrated in [4]. It was established that a 2.8 dB power gain may be achieved by optimal matching at the cost of higher correlation. Later, a closed form expression was derived for optimum matching impedance in terms of capacity at high signal-to-noise ratios (SNRs) [5]. A method for calculating the antenna radiation patterns based on the impedance matching network state was formulated in [6] for a MIMO system setup. However, these early studies do not consider user effects, realistic terminal antennas or diverse propagation scenarios.

A number of other contributions deal more explicitly with the propagation environment as part of the MIMO system performance evaluation [7]-[9]. In [7], reception of correlated fields from two closely spaced dipoles was studied in terms of received power, correlation and capacity. The simulation study showed that capacity gains from several matching conditions differed significantly for two different propagation channels, with uniform 2D angular power spectrum (APS) and a Laplacian 2D APS, respectively. Further studies in [8] and [9] that involved three-element arrays revealed that allowing the matching states to differ across the antenna elements can offer substantially larger performance gains. Moreover, simulation results of capacity using different propagation environments in [9] showed that for low SNR or high mutual coupling, active matching outperforms passive (or fixed) matching due to beamforming gains. However, for moderate coupling or high SNR, passive impedance matching enables better use of the multiple communication modes. Nevertheless, these studies considered only simple dipole antenna arrays, with no user.

More recent studies have used both measured and simulated results to verify the potential prospects of improving system performance with adaptive impedance matching (AIM) networks [10]-[15]. In [10] and [11], the tuning range and user influence of a reconfigurable PIFA with a fixed capacitor is presented. A relatively wide tuning range was shown in [10], whereas "soft" and "firm" one-hand grips were simulated in

Manuscript received June 30, 2014; revised October 28, 2015; accepted December 29, 2015. This work was supported in part by VINNOVA under grant no. 2009-02969, and in part by Vetenskapsrådet under grant no. 2010-468. This paper was presented in part at the 2013 IEEE International Symposium on Antennas and Propagation, Orlando, FL, USA, Jul 7-13, 2013.

I. Vasilev and B. K. Lau are with the Department of Electrical and Information Technology, Lund University, 221 00 Lund, Sweden (e-mail: {Ivaylo.Vasilev, Buon_Kiong.Lau}@eit.lth.se).

V. Plicanic is with the Network Technology Laboratory, Sony Mobile Communications AB, 221 88 Lund, Sweden (email: Vanja.Plicanic Samuelsson@sonymobile.com).

[11]. It was found that the user caused significant detuning in the low-Q antenna while minor deviations in performance were observed for the high-Q antenna. In [12], the indoor channel measurements performed for a dual-antenna mobile terminal in a two-hand user grip established that AIM can improve capacity performance by up to 44%, relative to 50 Ω terminations. Nonetheless, only one prototype and one user grip were investigated, and no actual tuners are used. Further measurements involving both indoor and outdoor scenarios are reported in [13], where mechanical tuners were utilized to experimentally verify AIM gains predicted from post-processing of channel data. An adaptive tuning module presented in [14] was tested with three commercial phones where severe mismatches between antennas and PAs were significantly improved highlighting the need of adaptive tuning solutions in current mobile devices. Nevertheless, only one APS was measured and non-standardized phantoms were used. In [15], three prototypes with significantly different properties were simulated with wideband adaptive tuning networks. The study focused on the effectiveness of AIM in compensating for user effects on the antenna bandwidth and impedance matching of these terminals. Yet, only uniform 3D APS was studied and there was no experimental verification.

In the context of the previous work, this paper makes the following contributions:

- The AIM performance of two fundamentally different MIMO antennas was investigated in three measured user scenarios, with four propagation environments added in post-processing. A detailed parametric study on the influence of the channel on AIM gains was performed.
- The physical mechanisms underlying the performance gains with AIM were identified and described. Based on ideal AIM, capacity gains between 1.3% and 44% were recorded depending on the antenna design, the user scenario and the propagation channel. The presence of losses in real AIM circuits and its implications on the results obtained with ideal AIM were also discussed.
- An exhaustive search over 9216 impedance matching states was done to determine the optimal capacity state. It was found that it involved a tradeoff between the related parameters of received signal power and correlation confirming results in the more limited study in [12].
- Based on these findings, several guidelines were formulated for designing AIM-enabled MIMO terminal antennas that provide robust capacity performance.

As the first study on the impact of terminal antenna design on MIMO performance in different user and propagation scenarios, the AIM system employed in this paper is assumed to be able to perfectly detect the scenarios, calculate/apply the optimal matching states and track non-stationary scenarios. Specifically, the AIM system consists of tunable lossless matching circuits and a custom designed MATLAB tool. The tool determines the optimal matching states by an exhaustive search based on the perfectly detected channel data of the given scenario. As such, the AIM system can be seen as an ideal closed loop system that can precisely track the optimal states in a single step for each new channel data in a non-stationary scenario.

The paper is structured as follows. Section II summarizes the system model adopted. Section III describes the two dual-antenna mobile terminals. Section IV presents the main results from the AIM studies in different user and propagation scenarios, whereas Section V gives the conclusions.

II. System Setup and Performance Metrics

A. System Model

In this study, the Kronecker model [16] is used to provide the end-to-end physical channel for MIMO communications, from which system performance such as capacity and multiplexing efficiency (ME) [17], [18] can be evaluated. Though simple in form, the Kronecker model has been found to be adequate for representing 2 × 2 MIMO channels [19]. We focus on the application of AIM in mobile terminals on the downlink, due to the stronger interest to increase data rates in the downlink. Therefore, for convenience, the correlation at the transmit antennas (at the base station) is assumed to be zero. Then, the end-to-end channel is only influenced by the propagation environment at the receiving end and the receiving antennas equipped with an AIM network at each port, as illustrated in Fig. 1. The channel is then given by [17]

$$\mathbf{H} = \mathbf{R}^{1/2}\mathbf{H}_w, \tag{1}$$

where $\mathbf{R} = \mathbf{\Lambda}^{1/2}\bar{\mathbf{R}}\mathbf{\Lambda}^{1/2}$ is the receive covariance matrix, $\mathbf{H}_w$ is a 2 × 2 matrix with independent and identically distributed (IID) complex Gaussian random variables, $\bar{\mathbf{R}}$ is a matrix with ones on the main diagonal and the antenna complex correlation coefficient as the off-diagonal terms and $\mathbf{\Lambda}$ is a diagonal matrix with the ith diagonal element representing the total antenna efficiency (or mean effective gain for channels with non-uniform APS [18]) of the ith antenna.

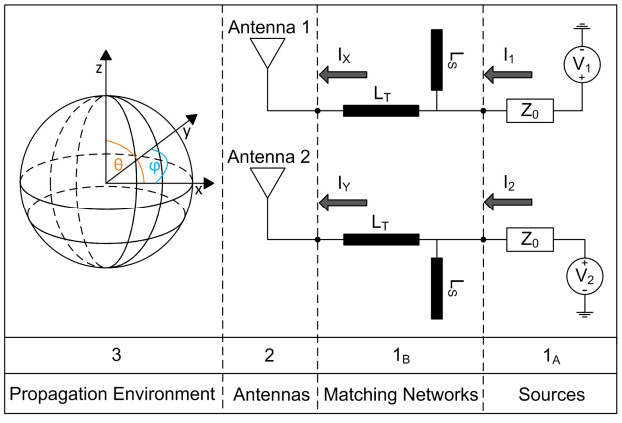

Fig. 1. Block diagram of the system model for AIM performance evaluation.

In general, when connected to the antennas, the AIM networks can modify the effective antenna patterns as seen at their output ports. Given the embedded antenna patterns, as well as the antenna scattering (S) parameters and the AIM matching state, the effective antenna patterns (and hence **R**) can be calculated [6]. The effective antenna patterns, derived for the transmitting case, are equal to those for the receiving case by reciprocity. It is noted that an embedded antenna pattern is obtained for a given antenna port, with other ports terminated in a reference impedance (i.e., 50Ω in this study).

To obtain the effective antenna pattern of a given antenna in the two-antenna setup illustrated in Fig. 1, the following procedure can be applied:

Step 1: *Excite the voltage source for the antenna under test*
For example, when port one is excited, $\mathbf{V} = [V_1 \quad V_2]^T$, $V_1 = 1$ V and $V_2 = 0$ V, where $(\,)^T$ denotes matrix transpose. Hence, when one of the antennas is active, the other one is terminated by the source impedance ($Z_0 = 50\ \Omega$).

Step 2: *Compute the source currents* $\mathbf{I} = [I_1 \quad I_2]^T$
This is achieved by first calculating the equivalent two-port transmission (ABCD) matrix representation [20] of the network as seen by the voltage sources

$$\mathbf{T} = \mathbf{T}_S \mathbf{T}_{M1} \mathbf{T}_A \mathbf{T}_{M2} \mathbf{T}_S, \tag{2}$$

where $\mathbf{T}_S$, $\mathbf{T}_{M1}$, $\mathbf{T}_{M2}$ and $\mathbf{T}_A$ are the transmission matrices of the sources, uncoupled matching networks (1 and 2), and antenna, respectively. Then, $\mathbf{T}$ is transformed into the Z-matrix representation $\mathbf{Z}$, and the currents are obtained using

$$\mathbf{I} = \mathbf{Z}^{-1}\mathbf{V}, \tag{3}$$

where $(\,)^{-1}$ denotes matrix inversion.

Step 3: *Compute induced current matrix* $\mathbf{A}$
The matrix $\mathbf{A}$ is based on the currents induced in the antenna elements and can be computed based on the S parameters of the antenna system $\mathbf{S}$. A detailed derivation of $\mathbf{A}$ can be found in [6]. In (4) and (5), U_0 is the magnitude of the excitation sources ($U_0 = 1$ V for simplicity), Z_0 is the transmission line characteristic impedance ($Z_0 = 50\ \Omega$), $\mathbf{I}_2$ is the 2×2 identity matrix. The voltages at the antenna ports $\mathbf{V}_G$ are obtained as

$$\mathbf{V}_G = \frac{U_0}{2}(\mathbf{S} + \mathbf{I}_2), \tag{4}$$

$$\mathbf{A} = Z_0 (U_0 \mathbf{I}_2 - \mathbf{V}_G)^{-1}. \tag{5}$$

Step 4: *Compute currents* I_X *and* I_Y
The currents I_X and I_Y at the antenna ports 1 and 2 can be calculated as follows:

$$\begin{bmatrix} V_X \\ I_X \end{bmatrix} = \mathbf{T}_X^{-1} \begin{bmatrix} V_1 \\ I_1 \end{bmatrix}, \tag{6}$$

$$\begin{bmatrix} V_Y \\ -I_Y \end{bmatrix} = \mathbf{T}_Y^{-1} \begin{bmatrix} V_1 \\ I_1 \end{bmatrix}, \tag{7}$$

where $\mathbf{T}_X = \mathbf{T}_S \mathbf{T}_{M1}$ and $\mathbf{T}_Y = \mathbf{T}_S \mathbf{T}_{M1} \mathbf{T}_A$ (8)

Step 5: *Compute effective radiation pattern*
The effective antenna pattern of port 1 (assuming $V_1 = 1$ V and $V_2 = 0$ V) is given by

$$E_{eff1}(\phi,\theta) = [\alpha \quad \beta] \begin{bmatrix} E_1(\phi,\theta) \\ E_2(\phi,\theta) \end{bmatrix}, \tag{9}$$

where

$$\begin{bmatrix} \alpha \\ \beta \end{bmatrix} = \mathbf{A} \begin{bmatrix} I_X \\ I_Y \end{bmatrix}, \tag{10}$$

$E_1(\phi,\theta)$ and $E_2(\phi,\theta)$ are the embedded antenna patterns of ports 1 and 2, respectively. $E_{eff2}(\phi,\theta)$ can be derived using the same procedure by setting $V_1 = 0$ V and $V_2 = 1$ V.

B. Simulation Setup

As depicted in Fig. 1, the system model of the terminal antenna with AIM in a propagation channel can be represented by three main blocks:

1) Variable Impedance Matching Network: To investigate the antenna performance under different matching conditions, we use a lossless network consisting of an open-circuited stub and a transmission line (Fig. 1). Assuming that the stub and transmission line can have variable dimensions (e.g., as in mechanical tuners [13]), the entire Smith chart can be covered with a predefined resolution depending on the time requirements for the simulation runs. Thus, we are able to exhaustively test all possible matching states. Figure 2 presents a complete sweep of the entire Smith chart with 96 matching states per port (i.e., $96^2 = 9216$ possible states for the two-port setup). The moderate number of states considered is an attempt to emulate the practical limitation of real AIM networks [21]-[26]. Nevertheless, the results presented in this contribution have been verified with a matching state grid of finer resolution. A finer grid was designed for each specific user and prototype case to provide a 10-fold increase in the number of states around the optimal matching states of the original grid. The optimal states in each case (over two ports) were the ones to provide maximum capacity at the center frequency. Only marginal improvements in performance of up to 3% were observed for the finer grid, which have no impact on the discussions and main conclusions of this paper.

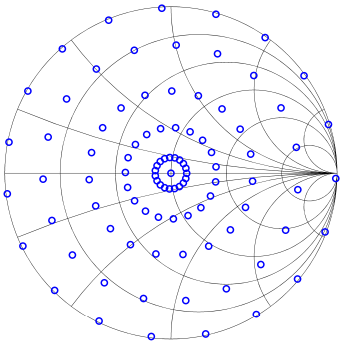

Fig. 2. Matching states used in the study.

2) Antenna Elements: This block represents the antenna elements in the mobile handset, as well as the user interaction in the nearfield. To obtain more realistic results, measured antenna scattering parameters and antenna patterns of fabricated prototypes were used, without and with user interactions (further details provided in Sections III and IV).

3) Propagation Environment: The last block represents the propagation environment. According to [27], different propagation environments can be characterized with different angular spreads. Thus, in addition to the uniform propagation environment, we account for various realistic propagation environments by limiting the angular spread of the incoming multipath components. Specifically, we assume an APS with truncated Gaussian distribution in both elevation and azimuth angles [18]. Moreover, the cross-polarization ratio (*XPR*) is assumed to be 0 dB in all the cases examined.

C. Figures of Merit

The main results in this contribution are discussed in terms of MIMO channel capacity and multiplexing efficiency (ME). For a 2 × 2 MIMO system the channel capacity with no channel state information at the transmitter [18] is

$$C = \log_2 \det\left(\mathbf{I}_2 + \frac{\rho_T}{2} \mathbf{H}\mathbf{H}^H \right), \quad (11)$$

where $\mathbf{I}_2$ is the 2 × 2 identity matrix, ρ_T is the SNR at the transmitter and $\mathbf{H}$ is the MIMO channel matrix defined in (1).

ME describes the additional power required for a practical MIMO antenna to achieve the same capacity as an ideal MIMO antenna with 100% total efficiency and zero correlation, for a given APS [18]. Hence, it can translate any impact on capacity performance into an equivalent power measure, which can be more intuitive. For high SNR (or high ρ_T), ME can be simplified to [18]

$$\eta_{ME} = \sqrt{\gamma_1 \gamma_2 \left(1 - |r|^2\right)}, \quad (12)$$

where r is the complex correlation coefficient between the two antennas for the given APS and

$$\gamma_i = 2\eta_i MEG_i, \quad (13)$$

where η_i and MEG_i are the ith antenna's total antenna efficiency and mean effective gain [27] in the given APS, respectively. The factor of 2 normalizes γ_i to 1 for 100% total efficiency and uniform 3D APS (i.e., $MEG_i = 0.5$). The expression (12) conveniently allows the impact of gain $(\gamma_1\gamma_2)^{1/2}$ and correlation $(1-|r|^2)^{1/2}$ to be studied separately.

III. MIMO Prototypes and User Scenarios

This section presents the two mobile terminal prototypes and the three user scenarios investigated in this study. Antenna radiation patterns and antenna total efficiencies were measured with a SATIMO Stargate 64 system [28], whereas a vector network analyzer was used to measure the S parameters. Both prototypes were designed to cover both LTE Band 18 (815-875 MHz) and LTE Band 9 (1.75-1.88 GHz). In this work, we focused only on LTE Band 18, since the lower band is more challenging for multi-antenna implementation.

A. User Scenarios

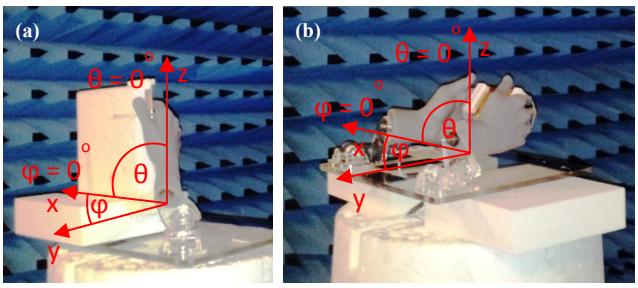

Fig. 3. User scenarios in the SATIMO Stargate 64 measurement system: (a) one-hand data mode (OH) and (b) two-hand data mode (TH). The reference coordinate system of the pattern measurements is also shown.

Three user scenarios were included in this study: free space (FS), one-hand data mode (OH) and two-hand data mode (TH). Figure 3 shows the OH and TH cases. The phantom hands were provided by IndexSAR [29]. The OH and TH cases were chosen to be representative of current terminal usage for browsing and data transfer. The positioning of the hands follows existing studies on user effects in terminal performance [12], [30].

B. MIMO Prototypes

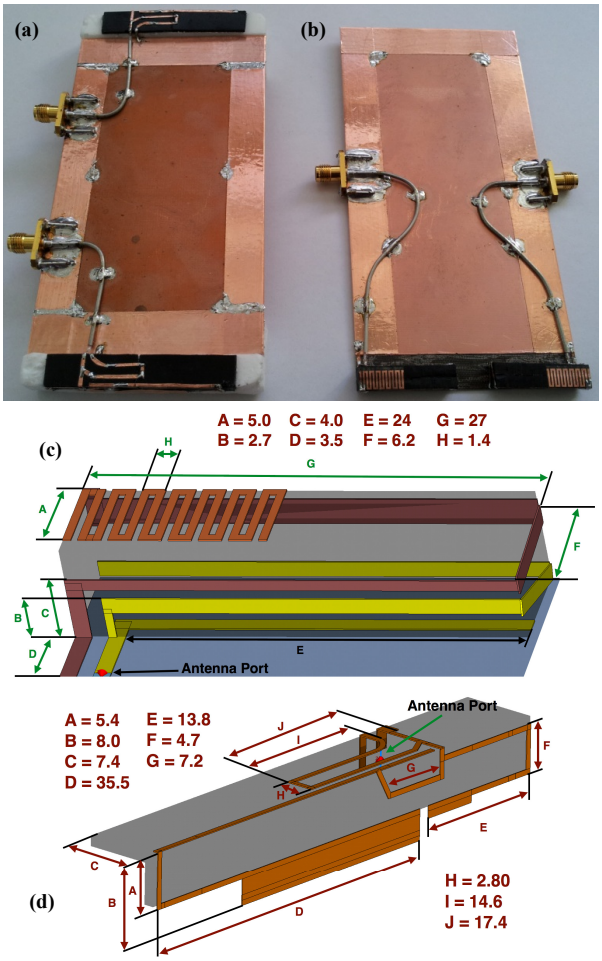

Fig. 4. Photo of (a) Prototype A and (b) Prototype B; Dimensions (in mm) of antenna element for (c) Prototype B and (d) Prototype A.

The terminal prototype in Fig. 4(a) (Prototype A) is based on [31] and comprises two compact dual-band inverted F antennas (IFAs) of an identical design. Each IFA element has the volume of 50 × 8 × 8 mm^3 (48 × 9 × 9 mm^3 fabricated, with minor retuning). The total volume of the prototype is 130 × 66 × 8 mm^3 (130 × 66 × 9 mm^3 fabricated). Copper (conductivity, σ = 5.8e7 S/m), FR4 substrate (relative permittivity, ε_r = 4.8) and plastic antenna carriers (ε_r = 2.7) were used to manufacture the terminal. The measured 6 dB impedance bandwidth is 85 MHz and 200 MHz at the lower and higher band, respectively (see Fig. 5). The average measured antenna isolation, total efficiencies and envelope correlation in FS over 860-875 MHz are -5.7 dB, -4.2 dB/-3.6 dB (port 1/port 2) and 0.38, respectively. Figures 5, 6 and 7

show the measured S parameters of Prototype A (PA) in the FS, OH and TH scenarios, respectively. The antenna radiation patterns for all three user scenarios are presented in Fig. 8. Moreover, to illustrate the relative positions of the antennas and the hand(s) in both simulation and measurement, 3D models for Prototype A in the three user scenarios and the corresponding coordinate system are shown in Fig. 8.

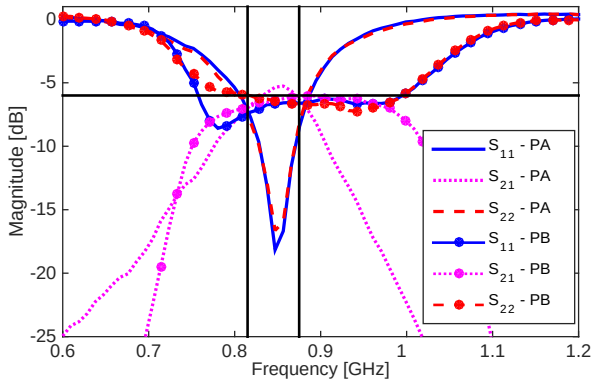

Fig. 5. Measured S parameters of Prototypes A and B in FS.

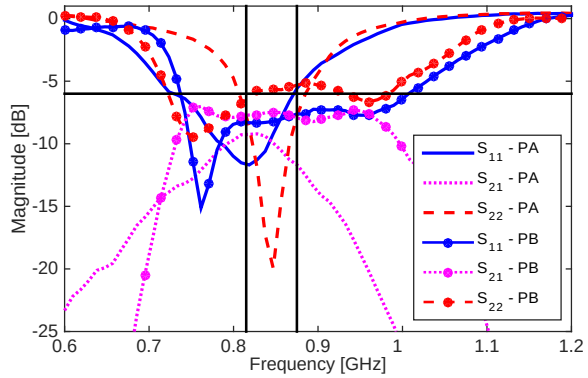

Fig. 6. Measured S parameters of Prototypes A and B in OH data mode.

Prototype B as shown in Fig. 4(b) is based on [32] and comprises of two compact dual-band monopole antennas of an identical design. The antenna elements consist of a two-branch feeding element along with a parasitic element extended from the ground plane for dual-band excitation. Each antenna occupies $27\times6\times7$ mm^3, ($27\times7\times7$ mm^3 fabricated, with minor retuning) and the total volume of the prototype is $130\times66\times7$ mm^3 . Copper (σ = 5.8e7 S/m), teflon substrate (ε_r = 2.54) and plastic antenna carriers (ε_r = 4.4) were $_{\text{used}}$ to manufacture the terminal. The 6 dB impedance bandwidth is 200 MHz at the lower band and 500 MHz at the higher band (see Fig. 5). The average measured antenna isolation, total efficiencies and envelope correlation in FS over 860-875 MHz are -6.2 dB, -4.5 dB/-4.2 dB (port 1/port 2) and 0.65, respectively. Figures 5, 6, and 7 show the measured S parameters of Prototype B (PB) in the FS, OH, and TH scenarios, respectively. The antenna patterns for all three user scenarios are presented in Fig. 9. Similar to Fig. 8, 3D models of Prototype B in the user scenarios are provided in Fig. 9. It is noted that the relatively low measured total efficiencies of Prototypes A and B (see Table I) are due to the mismatch/coupling losses of between -2.7 dB and -1.8 dB, as well as radiation efficiencies of between -2.3 dB and -1.5 dB. The measured radiation efficiencies were 0.7 – 1.3 dB lower than simulated values, which can be mainly attributed to the use of ferrite rings in the feed cable. Whereas the ferrites effectively mitigate leakage current to minimize radiation pattern distortion, it incurred additional losses [33].

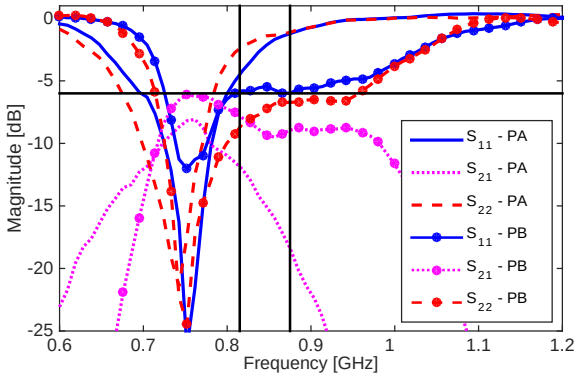

Fig. 7. Measured S parameters of Prototypes A and B in TH data mode.

IV. Results and Analysis

A. Uniform 3D APS

In this subsection, we show results on the AIM gains of the two prototypes in uniform 3D APS and explain the governing mechanisms behind the observed performance improvements. The results establish that AIM systems with uncoupled matching networks can improve antenna correlation at the price of lower antenna efficiencies when MIMO capacity is optimized. Moreover, some of the major observations in [12] and [15] were confirmed and extended. It was established that AIM heavily depends on antenna design and therefore on the interplay of key antenna characteristics such as correlation, isolation, bandwidth and impedance matching in FS. State-of-the-art AIM tuners are discussed in order to confirm the practicality of AIM systems in the presence of tuner insertion loss. Finally, the discussions in this subsection lead to the proposal of a novel terminal antenna design approach.

TABLE I
TOTAL EFFICIENCY, ENVELOPE CORRELATION, CAPACITY AND ME RESULTS FOR PROTOTYPES A AND B AVERAGED OVER LTE BAND 18 DOWNLINK (860-875 MHZ) FOR FS, OH AND TH SCENARIOS

User Case / Metric		Prototype A		Prototype B	
		50 Ω	**AIM**	**50 Ω**	**AIM**
FS	η_1 [dB]	-4.16	-4.42	-4.49	-5.53
	η_2 [dB]	-3.64	-3.72	-4.16	-5.11
	ρ_e	0.38	0.26	0.65	0.10
	Capacity [bits/s/Hz]	8.4	8.5	7.6	7.9
	Capacity gain	1.3%		4%	
	ME gain [dB]	0.2		1.1	
OH	η_1 [dB]	-8.49	-7.49	-7.31	-6.97
	η_2 [dB]	-3.80	-3.51	-6.21	-5.13
	ρ_e	0.04	0.03	0.41	0.22
	Capacity [bits/s/Hz]	7.6	8.0	6.8	7.4
	Capacity gain	5%		9%	
	ME gain [dB]	0.7		1.3	
TH	η_1 [dB]	-7.81	-3.98	-4.70	-4.19
	η_2 [dB]	-9.79	-5.28	-6.36	-5.66
	ρ_e	0.43	0.18	0.40	0.23
	Capacity [bits/s/Hz]	5.7	8.2	7.4	7.9
	Capacity gain	44%		8%	
	ME gain [dB]	5.0		1.1	

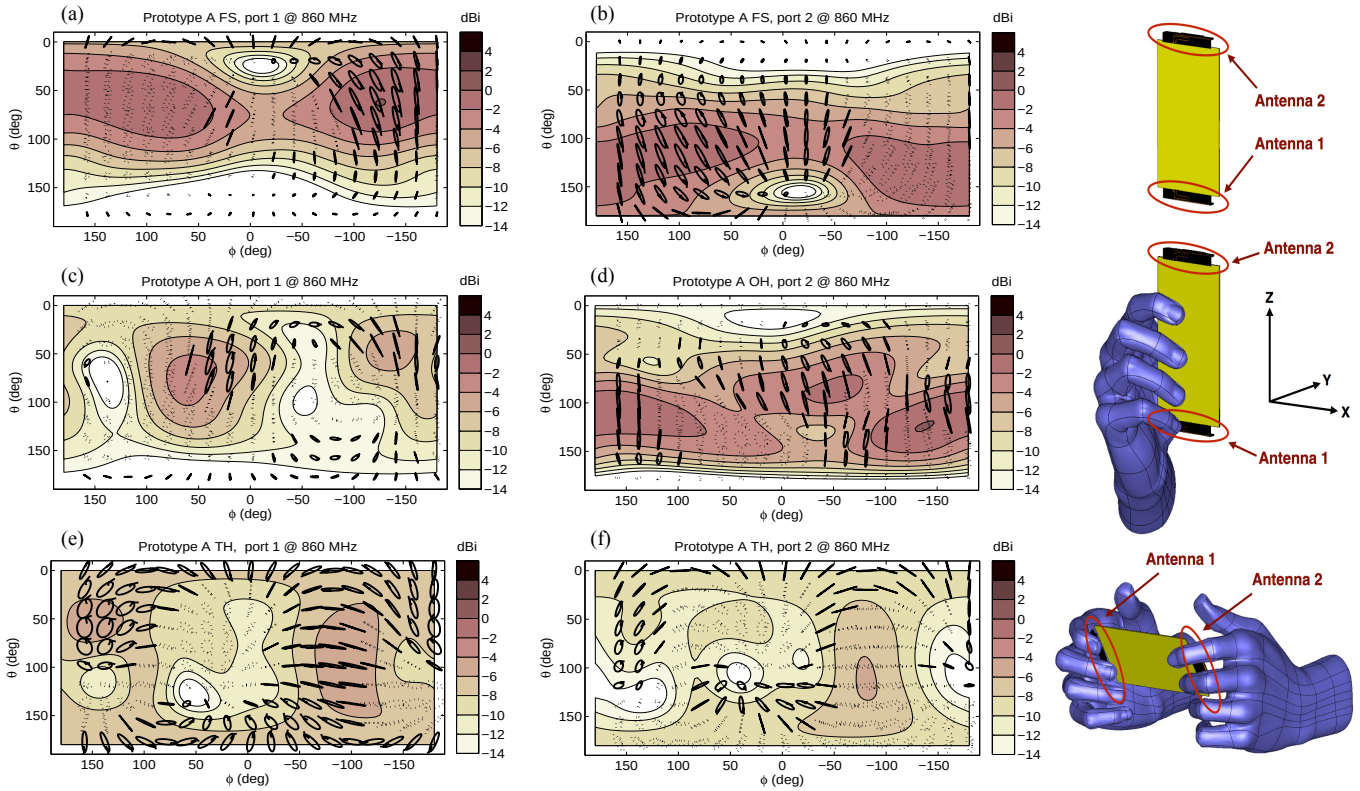

Fig. 8. Prototype A's 2D presentation of measured 3D radiation pattern and polarization states (dotted line circles = left hand circular polarization (LHCP), solid line circles = right hand circular polarization (RHCP)) of the two ports for FS (subplots (a)-(b)), OH (subplots (c)-(d)) and TH (subplots (e)-(f)) at 860 MHz; Illustrations of hand position with respect to the antenna elements in all three scenarios based on 3D models of the terminal (right side).

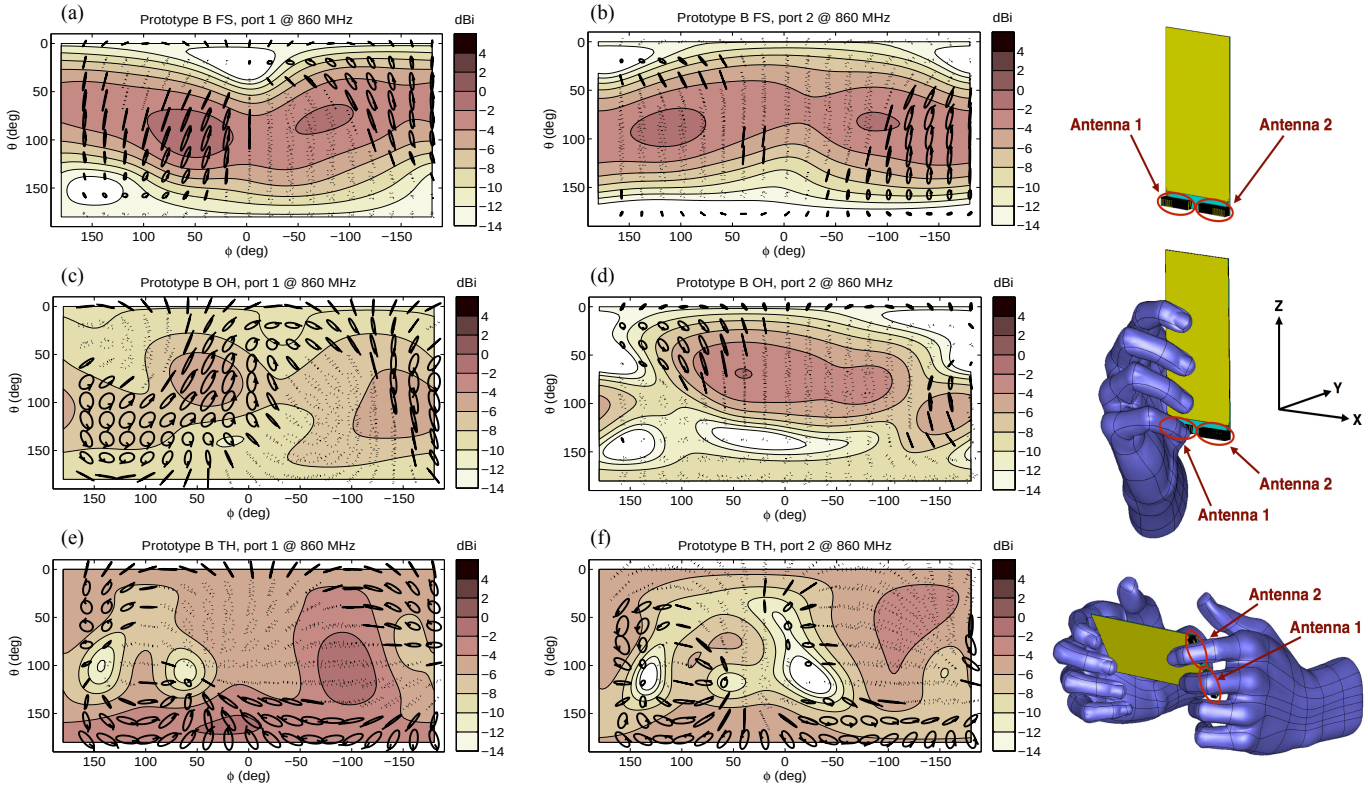

Fig. 9. Prototype B's 2D presentation of measured 3D radiation pattern and polarization states (dotted line circles = left hand circular polarization (LHCP), solid line circles = right hand circular polarization (RHCP)) of the two ports for FS (subplots (a)-(b)), OH (subplots (c)-(d)) and TH (subplots (e)-(f)) at 860 MHz; Illustrations of hand position with respect to the antenna elements in all three scenarios based on 3D models of the terminal (right side).

Table I presents capacity, efficiency, correlation and ME results for both prototypes in all scenarios (FS, OH and TH), averaged over three frequencies in LTE Band 18 Downlink (860, 867, 875 MHz), with the matching state optimized for capacity at the center frequency (867 MHz). Here, the capacity gain and ME gain show the improvement from employing AIM as compared to using standard 50Ω terminations. The reference SNR ρ_{T} is assumed to be 20 dB.

1) FS Performance

The S parameters in Figs. 5-7 as well as the results in Table I reveal four key design differences between the two prototypes (impedance matching, bandwidth, correlation and in part isolation). Prototype A offered 5.7 dB average isolation and a 6 dB bandwidth of 85 MHz in the lower frequency band, as compared to the 6.2 dB isolation and 200 MHz bandwidth offered by Prototype B. Nevertheless, the better bandwidth and isolation performance of Prototype B were achieved at the cost of poorer impedance matching and envelope correlation in FS (see Fig. 5-7 and Table I). In addition, Prototype B has a lower total efficiency compared to Prototype A.

These differences result in a higher capacity for Prototype A vs. Prototype B (8.4 bits/s/Hz vs. 7.6 bits/s/Hz). Applying AIM resulted in marginal improvements in capacity for both terminals in FS. Consistent with the indoor measurements in [12], the improved capacity performance involves a tradeoff between correlation and efficiency. When AIM is employed, the correlation for Prototype B is drastically reduced from 0.65 to 0.1. Using the concept of ME expressed by (12) [18], the drop in correlation is equivalent to a power gain of 2.1 dB. In contrast, the antenna efficiency is reduced by 1.0 dB on average across the two ports. Hence, when the capacity is optimized with the AIM system in this case, the total efficiency is sacrificed for a much lower correlation. A similar effect is observed for Prototype A, though to a smaller degree.

2) Effects of User Interactions

Due to absorption and mismatch losses, the OH scenario incurs capacity degradations of 0.8 bits/s/Hz both for Prototype A and Prototype B, relative to FS. Employing AIM leads to a marginal capacity gain for Prototype A (5%), whereas Prototype B shows a more promising result (9%). In Table I, we observe that the main contribution to the capacity gain in the case of Prototype A is the improved antenna efficiencies rather than improved correlation. Using (12), we can isolate the effects of correlation $(1-|r|^2)^{1/2}$ and efficiency (or gain) $(\gamma_1\gamma_2)^{1/2}$ on ME. The results suggest that, in the case of Prototype A, compensation of antenna mismatch offers ~0.64 dB to the gain in ME, whereas the correlation change contributes only ~0.02 dB. Hence, in this case the AIM gain is mainly due to mismatch loss compensation. On the other hand, in the case of Prototype B, improvement is observed in both antenna efficiency and envelope correlation. In this case, the reduced correlation provides ~0.6 dB in the ME gain whereas mismatch compensation contributes with ~0.7 dB. Therefore, in this case the AIM gain results from both mismatch compensation and improved correlation.

The results of the OH scenario in Table I also highlight that the severity of user effects depends heavily on the antenna location relative to the hand. In particular, the total efficiencies of the two antennas in Prototype A differ by as much as 4.7 dB, since one antenna is located close to the palm, whereas the other antenna (see Fig. 8) is placed far from the hand grip. Different user effect on the antennas is also observed in Prototype B, though with a lower efficiency difference of 1.1 dB. This is because even though both antennas are located next to each other and close to the palm, one antenna is slightly more obstructed by the hand grip than the other.

The TH scenario incurs a more significant penalty on the FS capacity performance (i.e., 2.7 bits/s/Hz) than the OH case for Prototype A, since in this case both antenna elements are covered by the user hands (see Fig. 8). The capacity drop is due to the severely decreased antenna efficiencies and slightly increased antenna correlation. However, employing AIM leads to a large capacity gain of 44%. Here, antenna efficiency contributes with 4.2 dB in ME gain whereas correlation improvement gives a further 0.8 dB. This result confirms the initial analysis in [12], where it was suggested that the TH user scenario with AIM can give similar performance as the FS case. This is because the reduced coupling and correlation in the TH scenario (relative to FS) compensates for the absorption losses in the hands. The performance of Prototype B in the TH scenario follows similar trends to the OH case.

These results reveal that AIM has strong potential to compensate for user interactions through two primary mechanisms: i) counteract efficiency degradation by mismatch compensation, with no significant impact on correlation; ii) bring about improvement in both efficiency and correlation. Mechanism 2 is especially relevant for multi-antennas, as it demonstrates the feasibility for AIM to go beyond mismatch compensation of individual antenna elements towards addressing both mismatch and correlation of the overall antenna system. However, it should be noted that although correlation can be improved in OH and TH cases, the use of uncoupled matching networks in this study limits the improvement in correlation to about 0.8 dB in terms of ME gain [7]. This is because changes in correlation are caused by changes in the antenna patterns. In the case of uncoupled matching networks, pattern changes rely on mutual coupling, where the non-excited antenna element can be seen as a reactively loaded parasitic antenna [34]. However, the mutual coupling in these prototypes in OH and TH is not high enough to enable pattern changes that can give even lower correlation. In contrast, the higher coupling for Prototype B in FS enables the uncoupled AIM to reduce correlation more effectively and contributes to 2.1 dB in ME gain.

3) Effects of Antenna Design Parameters

In cases where the user is present, the impedance mismatch is primarily caused by a decrease in the resonant frequency [35]. Due to design differences (antenna location and type), the maximum user-induced frequency offset at the low band for Prototype A (100 MHz) is larger than that for Prototype B (30 MHz), allowing the latter to be more robust to user effects. Moreover, Prototype B also has a significantly larger antenna bandwidth than Prototype A, meaning that an offset in the center frequency will only affect a smaller portion of the entire

band. Therefore, AIM offers only up to 9% in capacity gain for Prototype B, especially since the evaluated frequency still falls within the band despite the frequency offset. The effect of bandwidth on the AIM performance of mobile terminals was also considered in an earlier study [15]. Even though the bandwidth of the prototypes used in the study in [15] was up to 40 MHz, similar conclusions were reached on the increased robustness and decreased AIM gain of wider-band designs.

Another major difference in the design of the two prototypes is the impedance matching in FS. In order to achieve a large bandwidth, Prototype B maintains a reflection coefficient of around -6 dB throughout the band. In contrast, Prototype A has a clear single-resonance behavior within the band, giving significantly better matching than -6 dB, except at the band edges. Consequently, AIM offers 1.1 dB ME gain for Prototype B in FS by decreasing correlation at the expense of lower efficiency, whereas it has little impact for Prototype A. Nevertheless, in the presence of user, Prototype A suffers from generally poorer matching due to its smaller bandwidth than Prototype B, which allows it to benefit from mismatch compensation with AIM, especially for TH.

Two other notable differences in the design of the two prototypes are antenna element isolation and envelope correlation. In FS, the isolation of 5.7 dB for Prototype A is slightly lower than that of Prototype B (6.2 dB), which only accounts for 3% difference in the total efficiency. However, Prototype B has significantly higher envelope correlation in FS (0.65) than Prototype A (0.38), under uniform 3D APS. It is noted that the opposite trends in isolation and correlation confirm recent results that the two factors may not be positively correlated in the presence of antenna losses [36].

When user interaction was introduced, the mutual coupling was reduced in all cases. However, the correlation either increased or decreased, depending on the location of the user with respect to the antennas. Symmetric cases such as Prototype A in TH show higher correlation as compared to FS (0.43 vs. 0.38). Asymmetric cases such as OH for both prototypes give lower correlation as compared to FS. In general, Prototype B benefits from reduced correlation with AIM, whereas the impact of AIM on correlation in Prototype A is more marginal, except for TH.

4) Effect of Losses in Real AIM Implementations

As opposed to the ideal AIM considered in this work, state-of-the-art AIM circuit implementations [21]-[26] are lossy. To evaluate the practicality of AIM with respect to existing AIM implementations, we focus on the equivalent power gain (i.e. ME gain) from AIM due to changes in both total efficiency and correlation. Assuming a uniform 3D APS, the largest AIM improvement is observed for Prototype A in TH, with a ME gain of 5 dB. In contrast, the highest ME gain for Prototype B is 1.3 dB for OH. In [25], a micro-electromechanical system (MEMS)-based AIM circuit suitable for handsets was presented. Transducer gain measurements at 850 MHz indicated complete tuner losses (including all switches and variable capacitors) of below 1 dB for VSWR lower than 4 (equivalent to a return loss of 4.4 dB). For VSWR lower than 5 (equivalent to a return loss of 3.5 dB) the tuner loss was below 1.5 dB. Therefore, using 1.5 dB as a conservative benchmark for Prototype A, where lower return losses (higher mismatch) were observed, a significant ME gain of up to 5-1.5 = 3.5 dB can still be achieved with real AIM circuits in the uniform 3D environment. Moreover, as will be discussed in Section IV-B, higher AIM gains are achievable in non-uniform propagation environments (see Fig. 10). However, the limited AIM gains for Prototype B imply that only marginal improvements can be expected for the wideband terminal with realistic AIM networks. Using 1 dB as a conservative benchmark for Prototype B, where a higher return loss (lower mismatch) is observed, net AIM gains of up to 1.3-1 = 0.3 dB are achievable. Moreover, in some cases where lower impedance mismatch (high return loss) is observed, such as Prototype A in FS (see Fig. 5), the tuner losses will lead to negative gains (losses) of up to 0.2-1 = -0.8 dB.

5) Novel Terminal Antenna Design Approach

Until recently, terminal antennas were designed and optimized for only the FS scenario. This criterion would put Prototype A ahead of Prototype B in capacity performance (8.4 vs. 7.6 bits/s/Hz), when no AIM was used. However, mobile operators today require terminal antennas to be tested with user interactions, to ensure that the antennas provide robust performance in the presence of a user. This requirement tips the balance in favor of Prototype B over Prototype A, since it was revealed that a wideband design can significantly increase the robustness of the antenna to user interaction, relative to a narrowband design (see Fig. 5-7), despite poorer matching and correlation performance over the operating band. Specifically, the capacity of Prototype A decreased by up to 2.7 bits/s/Hz with user interaction, relative to 0.8 bits/s/Hz for Prototype B.

When AIM is used, both prototypes offer similar capacity performance in all scenarios. However, the behavior of the impedance mismatch for a given user scenario differs between the two prototypes, with the narrowband Prototype A suffering from higher mismatch than the wideband Prototype B. Since the measured tuner losses in [25] increased as the required matching state moved away from the 50Ω state, a higher mismatch is expected to result in higher losses. Therefore, despite Prototype A being slightly ahead of Prototype B in capacity performance for all scenarios (with AIM), Prototype B gives a more stable performance in all scenarios and offers lower AIM losses. Moreover, the wideband Prototype B has the advantage of covering more cellular bands.

These results suggest a new approach to antenna design, both without and with AIM. Instead of optimizing antenna performance in FS, it is beneficial to consider user influences in the initial design and sacrifice FS antenna matching and correlation properties for larger bandwidth and greater robustness to user effects. Moreover, today's antenna requirements are given in terms of efficiency related metrics of Total Radiated Power (TRP) and Total Isotropic Sensitivity (TIS). In contrast, our work has shown that optimizing the capacity (i.e., directly related to data throughput) with AIM can involve a trade-off between efficiency and correlation, whereby efficiency can be sacrificed for a lower correlation.

B. Gaussian 3D APS

Even though uniform 3D APS is commonly used as a

reference environment, real cellular environments are often characterized by limited angular spread (AS) in the incoming power. For example, the measurement-based WINNER II channel model presents an overall AS of between 12° and 53° at the user side, depending on the chosen scenario [37]. Moreover, due to the automatic screen rotation feature in many mobile terminals today, the orientation of the mobile terminal can be considered to be arbitrary. Therefore, in the following discussion we present a study of non-uniform APS environments for three ASs (15°, 30°, 60°). For a given AIM state, MEG was calculated for each antenna using the corresponding effective antenna pattern (obtained with the procedure in Section II-A) and the Gaussian APS in both azimuth and elevation planes according to [27] and [38], with XPR = 1 (0 dB). The modified MEG (13) was then obtained using the MEG and the effective antenna efficiencies. This process was performed for three ASs as well as for a full sweep of all incident angles in elevation ($0° \leq \theta \leq 180°$) and azimuth ($-180° \leq \phi \leq 180°$). Similarly, the envelope correlation was computed for all ASs and mean incident angles based on the discussion in [38] where the Gaussian APS, the measured patterns (of both ports) and XPR=1 were used. The channel matrix **H** was then formulated for each APS environment (mean incident angle and AS) using the Kronecker model (1), with correlation and modified MEG as inputs [18]. 2000 independent channel realizations were used to obtain the average capacity per frequency [18], which averaged out small scale fading. As for uniform 3D APS, the capacity with AIM was optimized using exhaustive search over all possible states for the center frequency of LTE Band 18 Downlink (867 MHz), where the optimal states were calculated for each AS and mean incident angle. The optimal states at 867 MHz were used to calculate the modified MEG, correlation and average capacity at 860 and 875 MHz, taking into account S parameter and efficiency variations. Figure 10 summarizes the range of capacity gain in percentage with AIM over all incident angles in elevation and azimuth for the three scenarios (FS/OH/TH). The absolute capacity gains for different incident angles and ASs are shown for two scenarios in Fig. 11.

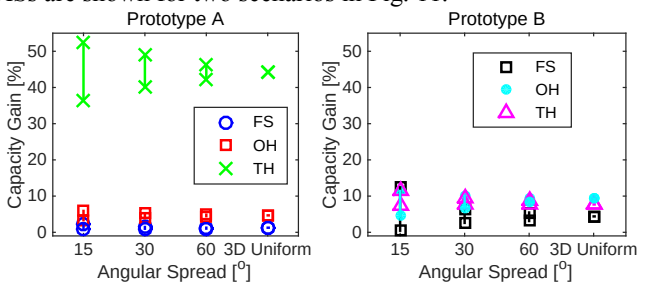

Fig. 10. Range of capacity gains from AIM in percentage over all incident angles for different ASs averaged over LTE 18 Downlink (860-875 MHz).

As depicted in Figs. 10 and 11, capacity gain can vary to some extent according to the AS and incident angle. In general, the range of capacity gains in each scenario, which is largest for AS = 15°, converges to the single number of the uniform 3D APS case as the AS increases. For example, a maximum gain of 52% at AS = 15° for Prototype A in TH, decreases to 46% at AS = 60°. Similarly, the gain of Prototype B in FS can be as high as 12% at AS = 15°, but only 6% at AS = 60° (vs. 4% for uniform 3D APS).

The variation in the capacity gain over incident angle in Fig. 11 reflects the extent to which AIM impacts upon the interaction between the narrow APS and the antenna patterns. For example, the absolute capacity gain maxima are located at ϕ = 60° and θ = 90° for Prototype A in OH in Fig. 11(a). Comparing this result with the corresponding antenna patterns in Fig. 8, it can be seen that the AIM gain maxima are located in close proximity to the radiation pattern maxima. It was also found that AIM has little impact on the correlation at these maxima (see Fig. 12), indicating that the antenna patterns were largely unaffected by AIM. Hence, the increased AIM gain is mainly due to increased total received power. Moreover, even though the antenna efficiency is increased, the focusing of the power at higher or lower gain region of the antenna pattern with narrow APS will result in power gain from AIM at different SNR levels. Due to the logarithmic dependence of capacity on SNR (see (11)), higher gain regions will thus offer higher absolute capacity gains. Therefore, when minor changes are seen in the correlation (see Fig. 12), regions of high AIM capacity gain will correspond to the antenna pattern maxima. Though not shown in this paper, similar observation has been made for Prototype B in TH.

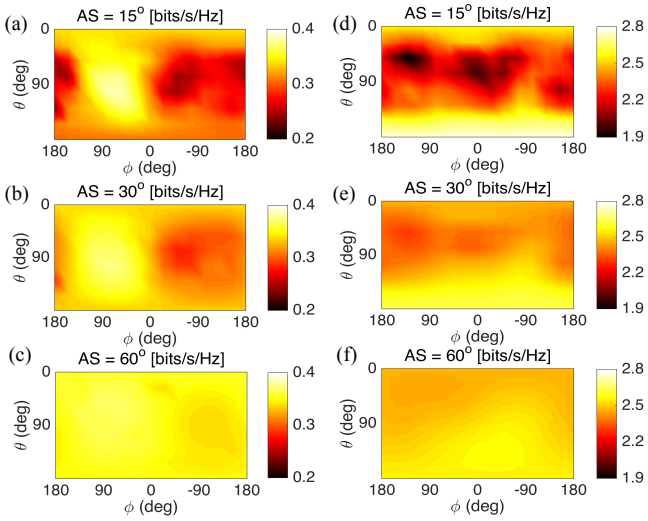

Fig. 11. Absolute capacity gain for Prototype A in OH (subplots (a)-(c)) and Prototype A in TH (subplots (d)-(f)) for AS = 15° (subplots (a) and (d)), AS = 30° (subplots (b) and (e)) and AS = 60° (subplots (c) and (f)) averaged over LTE 18 Downlink (860-875 MHz).

Nevertheless, in other cases such as Prototype A in TH, the spatial distribution of the correlation is affected by AIM. Therefore, the antenna pattern gain no longer dominates the AIM gain behavior. To illustrate this mechanism, Fig. 13 shows the MEGs (γ_1 and γ_2) and the envelope correlation over different incident angles for the optimal capacity match (AIM) and the 50Ω termination. The AIM gain result for Prototype A in TH (see Fig. 11(d)) indicates that the maximum gain is obtained for ϕ = 0°/180° and θ = 0°/180°. In contrast, the region of high MEGs for both antenna ports on Prototype A is around ϕ = -90° and θ = 90°. Moreover, it can be seen that the incident angles of maximum capacity gain coincide with low

correlation and high correlation gain from AIM. As a further confirmation, the minimum capacity gain in Fig. 11(d) is located at $\phi = 135°$ and $\theta = 45°$, which coincides with a region of high correlation and low correlation improvement from AIM. Therefore, in this case the capacity gain is significantly affected by correlation. Similar impact on capacity gain from correlation improvement was observed for Prototype B in OH.

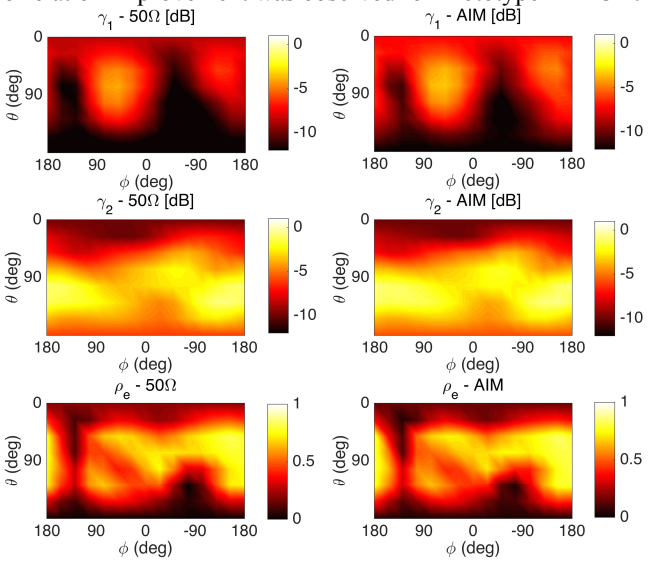

Fig. 12. MEGs (ports 1 and 2) and envelope correlation for 50 Ω termination and with AIM for Prototype A in OH and AS = 15° averaged over LTE 18 Downlink (860-875 MHz).

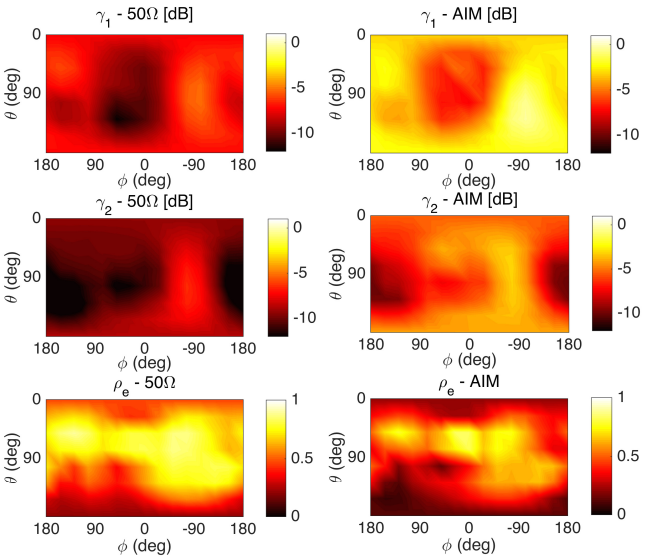

Fig. 13. MEGs (ports 1 and 2) and envelope correlation for 50 Ω termination and with AIM for Prototype A in TH and AS = 15° averaged over LTE 18 Downlink (860-875 MHz).

V. Conclusions

In this work, a framework for the capacity evaluation of AIM in MIMO terminals was presented. The evaluation was performed for two MIMO terminal prototypes in three user scenarios (FS, OH and TH) and four propagation conditions (uniform 3D APS and narrow APS with AS = 15°, 30°, and 60°). Antenna radiation properties for all user scenarios were measured in a SATIMO measurement system, whereas AIM and propagation channel were added in post-processing.

The results show that AIM has the potential to significantly improve terminal performance in many of the user and propagation scenarios tested. Capacity gains of up to 44% (or 5.0 dB in ME gain) can be achieved in uniform 3D APS, relative to 50Ω termination. As in the case of single-antenna terminals, the primary mechanism for AIM to bring about capacity gain is through compensating for the impedance mismatch from user interaction. However, AIM can also decrease the correlation in some cases, giving equivalent power gains of 2.1 dB in FS and up to 0.8 dB with user. In general, the ability of AIM to further decrease correlation can be achieved by the use of coupled AIM networks.

Antenna design parameters such as isolation, bandwidth and impedance matching were identified as key factors influencing the AIM performance, in addition to the location of the antenna relative to the user. It was shown that the terminal with good impedance matching in FS and narrower bandwidth (Prototype A) was more susceptible to user influence and hence obtained larger improvements from AIM. In contrast, the wideband terminal solution (Prototype B) was more robust to user influence (i.e., causing smaller mismatch), at the cost of poorer matching and higher correlation in FS. Since both designs achieve similar capacity with AIM, the wideband solution is preferred due to lower losses from compensating for a smaller mismatch in practical AIM circuits.

In this context, a new user-centric terminal antenna design approach was proposed, where impedance matching and correlation in FS are traded for increased robustness to user effects, larger bandwidth and lower AIM losses. The initial results presented suggested that the loss in FS performance is not as significant as the gain from user robustness. We therefore concluded that this strategy is a promising method for designing terminals that are robust over a wide range of user and propagation scenarios. It is also noteworthy that our approach of optimizing capacity, rather than only efficiency, has shown that a tradeoff between efficiency and correlation may be necessary to achieve the best MIMO performance.

Moreover, in non-uniform APS of limited angular spreads, the gain from AIM can be higher or lower than the uniform 3D APS case, due to the alignment between antenna patterns and the incident angle of the incoming power. The maximum capacity gain achieved with AS = 15° is 52% and 12% for Prototypes A and B, respectively. It was also found that in cases of low correlation changes from AIM, the maximum AIM gain corresponds to antenna pattern maxima, whereas in cases of high correlation changes due to AIM the maximum AIM gain depends on both the MEGs and the correlation.

Acknowledgment

The authors thank Prof. Henrik Sjöland of Lund University for helpful discussions, as well as Farzaneh Firouzabadi and Scott Vance of Sony Mobile Communications AB, Lund, Sweden for providing the design for Prototype B.

References

[1] F. Boccardi et al., "Multiple-antenna techniques in LTE-Advanced," *IEEE Commun. Mag.*, vol. 50, no. 3, pp. 114-121, Mar. 2012.

[2] B. K. Lau, "Multiple antenna terminals," in *MIMO: From Theory to Implementation*, C. Oestges, A. Sibille, and A. Zanella, Eds. San Diego: Academic Press, 2011, pp. 267-298.

[3] R. Vaughan and J. B. Andersen, *Channels, Propagation and Antennas for Mobile Communications*. London, U.K.: IEE, 2003.

[4] J. B. Andersen and B. K. Lau, "On closely coupled dipoles in a random field," *IEEE Antennas Wireless Propag. Lett*., vol. 5, pp. 73-75, 2006.

[5] Y. Fei et al., "Optimal single-port matching impedance for capacity maximization in compact MIMO arrays," *IEEE Trans. Antennas Propag.,* vol. 56, no. 11, pp. 3566-3575, Nov. 2008.

[6] K. Karlsson, "Embedded element patterns in combination with circuit simulations for multi-port antenna analysis," *PhD Thesis,* Department of Signals and Systems, Chalmers University of Technology, Gothenburg, Sweden*,* 2009.

[7] B. K. Lau, J. B. Andersen, G. Kristensson, and A. F. Molisch, "Antenna matching for capacity maximization in compact MIMO systems," in *Proc. 3rd Int. Symp. Wireless Commun. Syst. (ISWCS'2006)*, Valencia, Spain, Sep. 5-8, 2006, pp. 253-257.

[8] R. Tian and B. K. Lau, "Uncoupled antenna matching for performance optimization in compact MIMO systems using unbalanced load impedance," in *Proc. IEEE Veh. Technol. Conf. Spring (VTC Spring 2008)*, Singapore, May 11-14, 2008, pp. 299-303.

[9] M. Jensen and B. K. Lau, "Uncoupled matching for active and passive impedances of coupled arrays in MIMO systems," *IEEE Trans. Antennas Propag.*, vol. 58, no. 10, pp. 3336-3343, Oct. 2010.

[10] S. C. Del Barrio, M. Pelosi, O. Franek, and G. F. Pedersen, "Tuning range optimization of a planar inverted F antenna for the LTE low frequency bands," in *Proc. Veh. Technol. Conf. Fall (VTC Fall 2011),* San Francisco, CA, Sep. 2011.

[11] S. C. Del Barrio, M. Pelosi, O. Franek, and G. F. Pedersen, "The effect of the user's body on high-Q and low-Q planar inverted F antennas for LTE frequencies," in *Proc. Veh. Technol. Conf. Spring (VTC Spring 2012),*Yokohama, Japan, May 2012.

[12] V. Plicanic, I. Vasilev, R. Tian, and B. K. Lau, "Capacity maximisation of handheld MIMO terminal with adaptive matching in indoor environment," *IET Electron. Lett.,* vol. 47, no. 16, pp. 900-901, 2011.

[13] I. Vasilev, V. Plicanic, R. Tian, and B. K. Lau, "Measured adaptive matching performance of a MIMO terminal with user effects," *IEEE Antennas Wireless Propag. Lett*., vol. 12, pp. 1720-1723, 2013.

[14] K. R. Boyle, et al., "Gain statistics for mobile phone antenna tuners," in *Proc. Europ. Conf. Antennas Propag. (EuCAP'2013)*, Gothenburg, Sweden, Apr. 8-12, 2013, pp. 424-428.

[15] I. Vasilev, E. Foroozanfard, and B. K. Lau, "Adaptive impedance matching performance of MIMO terminals with different bandwidth and isolation properties in realistic user scenarios," in *Proc. Europ. Conf. Antennas Propag. (EuCAP'2013)*, Gothenburg, Sweden, Apr. 8-12, 2013, pp. 2516-2520.

[16] J. P. Kermoal et al., "A stochastic MlMO radio channel model with experimental validation," *IEEE J. Sel. Commun*., vol. 20, no. 6, pp. 1211-1226, Aug. 2002.

[17] R. Tian, B. K. Lau and Z. Ying, "Multiplexing efficiency of MIMO antennas," *IEEE Antennas Wireless Propag. Lett.,* vol. 10, pp.183-186, 2011.

[18] R. Tian, B. K. Lau and Z. Ying, "Multiplexing efficiency of MIMO antennas in arbitrary propagation scenarios," in *Proc. Europ. Conf. Antennas Propag. (EuCAP'2012)*, Prague, Czech Republic, Mar. 26-30, 2012, pp. 373-377.

[19] H. Özcelik et al., "Deficiencies of the Kronecker MIMO radio channel model," *IEE Electron. Lett*., vol. 39, no. 16, pp. 1209–1210, Aug. 2003.

[20] D. M. Pozar, *Microwave Engineering 3rd ed.,* U.S.A.: John Wiley & Sons, 2005.

[21] P. Sjöblom and H. Sjöland, "An adaptive impedance tuning CMOS circuit for ISM 2.4-GHz band," *IEEE Trans. Circuits Syst. I,* vol. 52, no. 6, pp. 1115-1124, Jun. 2005.

[22] P. Sjöblom and H. Sjöland, "Characterization of CMOS impedance tuning unit for DVB-H," *Analog Integrated Circuits and Signal Processing,* vol. 52, no. 3, pp. 79-87, Sep. 2007.

[23] Z. Popovic and L. Sankey, "Adaptive tuning for handheld transmitters" in *Proc. Microw. Symp. Digest (IEEE MTT 2009)*, Boston, MA, Jun. 7-12, 2009, pp. 225-228.

[24] K. R. Boyle, et. al., "Gain statistics for mobile phone antenna tuners," in *Proc. Europ. Conf. Antennas Propag. (EuCAP'2013)*, Gothenburg, Sweden, Apr. 8-12, 2013, pp. 424-428.

[25] A. S. Morris III, Q. Gu, M. Ozkar, and S. P. Natarajan, "High performance tuners for handsets," in *Proc. IEEE Microw. Theory Tech. Symp. (MTT'2011)*, Baltimore, MD, Jun. 5-10, 2011.

[26] R. Valkonen et al., "Frequency-reconfigurable mobile terminal antenna with MEMS switches," in *Proc. Europ. Conf. Antennas Propag. (EuCAP'2010)*, Barcelona, Apr. 12-16, 2010.

[27] T. Taga, "Analysis for mean effective gain of mobile antennas in land mobile radio environments," *IEEE Trans. Veh. Technol.,* vol. VT-39, no. 2, pp. 117-131, May 1990.

[28] [Online]. Available: http://www.satimo.com/content/products/sg-64

[29] [Online]. Available: http://www.indexsar.com/index-phantomhands.html

[30] M. Pelosi et al., "A grip study for talk and data modes in mobile phones," *IEEE Trans. Antennas Propag.,* vol. 57, no. 4, pp. 856-865, Apr. 2009.

[31] K. Ishimiya, "Multiband antenna device and communication terminal device," PCT Patent Application (WO/2007/049414 A1), May 3, 2007.

[32] W. Chen, and K. L. Wong, "Small-size coupled-fed shorted T-monopole for internal WWAN antenna in the thin-profile mobile phone," *Microw. Opt. Technol. Lett.,* vol. 52, no. 2, pp. 257-262, Feb. 2010.

[33] S. Zhang, B. K. Lau, A. Sunesson, and S. He, "Closely-packed UWB MIMO/diversity antenna with different patterns and polarizations for USB dongle applications," *IEEE Trans. Antennas Propag*., vol. 60, no. 9, pp. 4372-4380, Sep. 2012.

[34] H. Kawakami and T. Ohira, "Electrically steerable passive array radiator (ESPAR) antennas," *IEEE Antenna Propag. Mag.*, vol. 47, no. 2, Mag., pp. 43-49, Apr. 2005.

[35] P. Vainikainen, J. Holopainen and M. Kyro, "Antennas for digital television receivers in mobile terminals," *IEEE Proc.,* vol. 100, no. 7, pp. 2341-2348, Jul. 2012.

[36] H. Li, X. Lin, B. K. Lau, and S. He, "Equivalent circuit based calculation of signal correlation in lossy antenna arrays," *IEEE Trans. Antennas Propag*., vol. 61, no. 10, pp. 5214-5222, Oct. 2013.

[37] IST-WINNER D1.1.2 P. Kyösti, et al., "WINNER II channel models", ver 1.1, Sept. 2007. Available: https://www.ist-winner.org/WINNER2-Deliverables/D1.1.2v1.1.pdf

[38] M. B. Knudsen and G. F. Pedersen, "Spherical outdoor to indoor power spectrum model at the mobile terminal," *IEEE Journ, Selected Areas in Communications*, vol. 20, no. 6, pp. 1156-1169, Aug. 2002.

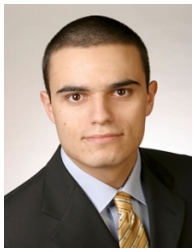

Ivaylo Vasilev (S'09) received the M.S. and the Ph. D. degrees in electrical engineering from Jacobs University, Bremen, Germany and Lund University, Lund, Sweden, in 2010 and 2015, respectively.

From 2009 to 2010, he was an embedded system engineer at microFAB GmbH in Germany where he worked towards the development of a MEMS pressure system targeting automotive applications. From 2010 to 2015 he pursued the Ph.D. degree at the Department of Electrical and Information Technology in Lund University working on the theoretical study and practical implementation of adaptive impedance matching for the realization of user robust MIMO terminal antennas. Ivaylo Vasilev is currently a System Engineer at Visteon Corporation. His research interests comprise RF and embedded systems and their implementation to novel scenarios.

Ivaylo Vasilev was an active contributor in the European research initiative COST IC 1004.

Vanja Plicanic (M'07) received the M.S. and the Ph. D. degrees in electrical engineering both from Lund University, Lund, Sweden, in 2004 and 2011, respectively.

From 2004 to 2005, she was a Young Graduate Trainee at the Antenna and Submillimetre Wave Group at European Space Research and Technology Centre, ESTEC in the Netherlands. In 2005, Vanja joined Sony Ericsson Mobile Communications (now Sony Mobile Communications) as RF engineer. From 2007 to 2014 she was a researcher in the Communications and Networking Group, focusing on smart antenna systems and their implementation in compact mobile devices. Vanja is now a senior researcher at Network Technology Lab at Research and Incubation, Sony Mobile. She shares her time between research on machine type communication and incubation lead for new businesses within the area of Internet of things (IoT).

Vanja Plicanic has participated in the European research initiative COST 2100 and has been member of Technical Program Committee for a number of conferences, latest being the 81st IEEE Vehicular Technology Conference VTC2015-Spring in Glasgow, Scotland. She has 20 filed patents within the area of network technologies.

Buon Kiong Lau (S'00–M'03–SM'07) received the B.E. degree (with honors) from the University of Western Australia, Perth, Australia, and the Ph.D. degree from the Curtin University of Technology, Perth, Australia, in 1998 and 2003, respectively, both in electrical engineering.

During 2000 to 2001, he was a Research Engineer with Ericsson Research, Kista, Sweden. From 2003 to 2004, he was a Guest Research Fellow at the Department of Signal Processing, Blekinge Institute of Technology, Sweden. Since 2004, he has been with the Department of Electrical and Information Technology, Lund University, where he is now an Associate Professor. He has been a Visiting Researcher with the Department of Applied Mathematics, Hong Kong Polytechnic University, China; the Laboratory for Information and Decision Systems, Massachusetts Institute of Technology, Cambridge, MA, USA; and the Takada Laboratory, Tokyo Institute of Technology, Japan. His primary research interests are in various aspects of multiple antenna systems, particularly the interplay between antennas, propagation channels, and signal processing.

Dr. Lau is a Senior Associate Editor for the IEEE TRANSACTIONS ON ANTENNAS AND PROPAGATION, for which he was a Guest Editor of the 2012 Special Issue on MIMO Technology and is the Lead Guest Editor of the upcoming 2016 Special Issue on Theory and Applications of Characteristic Modes. He was the Lead Guest Editor of the 2013 Special Cluster on Terminal Antenna Systems for 4G and Beyond for the IEEE Antennas and Wireless Propagation Letters. From 2007 to 2010, he was a Co-Chair of Subworking Group 2.2 on "Compact Antenna Systems for Terminals" (CAST) within EU COST Action 2100. From 2011 to 2015, he has been a Swedish national delegate and the Chair of Subworking Group 1.1 on "Antenna System Aspects" within COST IC1004. From 2012-2015, he was the Regional Delegate of European Association on Antennas and Propagation (EurAAP) for Region 6 (Iceland, Norway, and Sweden). He is also a member of the Education Committee within the IEEE Antennas and Propagation Society (AP-S), where he served as the Coordinator for the annual IEEE AP-S Student Design Contest from 2013 to 2015.

In 2015, Dr. Lau received an award from the IEEE TRANSACTIONS ON ANTENNAS AND PROPAGATION for exceptional performance as an associate editor.